Reports

Growth of Thin Chemically Bonded Diamondlike Films by Ion Beam Deposition

J. WAYNE RABALAIS AND SRINANDAN KASI

Carbon films with a diamondlike structure that are chemically bonded to surfaces have been deposited by means of low-energy C$^+$ ion beams. When mass-selected C$^+$ beams at energies in the range from 20 to 200 electron volts impinge on atomically clean surfaces, the first carbon monolayer grows as a carbide structure that is chemically bonded to the surface. As deposition continues, the structure evolves over the next several atomic layers into a diamondlike structure. These pure carbon films are strongly adhered to the surface through the carbide bonds, which also provide for an intimate interface. There are significant applications for such films, particularly as insulators and doped semiconductors.

THE ABILITY TO REPRODUCIBLY form thin carbon films with a diamond structure has important technological applications (*1*), not only because of the strength and hardness of diamond, but because it has an extremely low electrical conductivity (excellent electrical insulator) and has the highest thermal conductivity (excellent heat conductor) of all known substances (*2*). These properties stem from the strong, rigid, symmetrical tetrahedral bonding between carbon atoms. This bonding produces an extremely elastic lattice with low phonon amplitudes, that is, the thermal motions have limited amplitude; as a result, the diamond allotrope of carbon has the lowest specific heat of all elements and high heat transfer rates.

Diamondlike carbon films have been deposited previously (*3, 4*) by a variety of plasma deposition, chemical vapor deposition, and ion beam techniques. Progress in film growth technology has been impeded by a lack of reproducibility and by embedded impurities, both of which result from use of only moderate vacuum conditions and non-mass-selected hydrocarbon discharges as a source of carbon. We report the growth of pure carbon films in a diamondlike allotrope that are chemically bonded to the substrate surfaces.

A low-energy mass-selected C$^+$ ion beam (1 to 300 eV) was directed into an ultrahigh vacuum (UHV) chamber (10^{-10} torr) for carbon deposition onto an atomically clean substrate surface. The C$^+$ ions were produced at low energy in a Colutron ion source from carbon-containing gases that were accelerated to high velocity, mass-selected, focused, and decelerated prior to impact with the substrate. Four stages of differential pumping serve to maintain UHV conditions in the deposition chamber. The substrate surface was cleaned in situ by Ar$^+$ bombardment (10 μA/cm^2) and by annealing to high temperatures (~800°C) prior to deposition. In situ surface spectroscopic techniques such as x-ray and ultraviolet photoelectron spectroscopy (XPS and UPS), Auger electron spectroscopy (AES), and electron energy loss spectroscopy (ELS) as well as spectroscopic ellipsometry were used for characterization of the deposit. The apparatus has been described elsewhere (*5*).

Spectroscopic measurements were performed as a function of C$^+$ energy and dose and at the final "steady-state" conditions; these conditions were defined as the dose after which the detailed spectral features remained constant. Films were deposited on surfaces of Si(100), Ni(111), tantalum, tungsten, and gold with similar results in all cases; only selected examples of these are presented below. The spectroscopic measurements were compared to those made on a pyrolytic graphite sample in the same instrument and to published spectra of pure diamond (*6–10*).

The nature of the carbon deposit and the evolution of the film can be intimately followed by means of the carbon Auger line shape. These line shapes serve as a fingerprint of the chemical environment. The evolution of the C KLL Auger line shape as a function of C$^+$ dose on Ni(111) is shown in Fig. 1. For initial C$^+$ doses in the range $\sim 2 \times 10^{15}$ to 3×10^{15} ions per square centimeter, the line shape (Fig. 1a) corresponds to that of a carbide (Ni$_n$C). The deposit is approximately one monolayer thick at this stage. Figure 1b shows the line shape corresponding to a dose of $\sim 6 \times 10^{15}$ to 8×10^{15} ions per square centimeter, for which metal-carbon composite layers and three-dimensional carbon overlayers begin to grow. With additional C$^+$ deposition, structures characterized by the spectra in Fig. 1, c and d, develop. The line shape of Fig. 1c is similar to that of sp^2 hybridized graphite, whereas that of Fig. 1d is the characteristic signature of sp^3 hybridized diamond. The distinction between diamond and graphite allotropes is even more pronounced in the low-energy portion of the spectrum. Graphite spectra exhibit two peaks at ~80 and ~110 eV that are absent in diamond spectra. The broad Auger scans

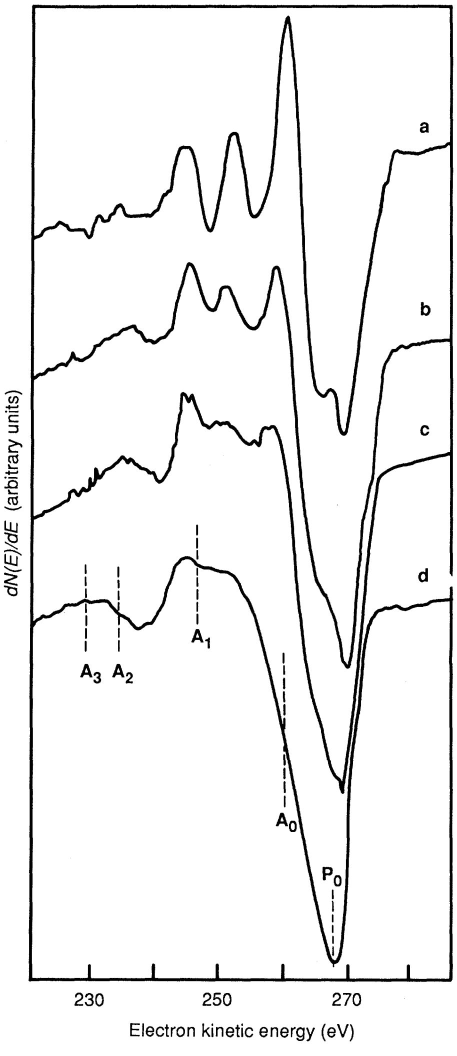

Fig. 1. Evolution of the AES line shape from carbidic to diamondlike structures for 75 eV C$^+$ deposition on Ni(111). The doses were: (**a**) 2.0×10^{15}, (**b**) 6×10^{15}, (**c**) 9×10^{15}, and (**d**) $> 2 \times 10^{16}$ ions/cm^2. P$_0$ represents the maximum negative excursion of the derivative and A$_0$ to A$_3$ represent inflection points in the derivative curve.

Department of Chemistry, University of Houston, Houston, TX 77004.

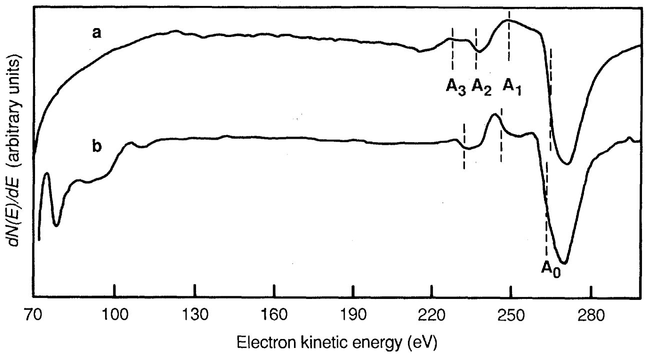

Fig. 2. AES spectra of (**a**) a deposited diamondlike film and (**b**) a graphite sample.

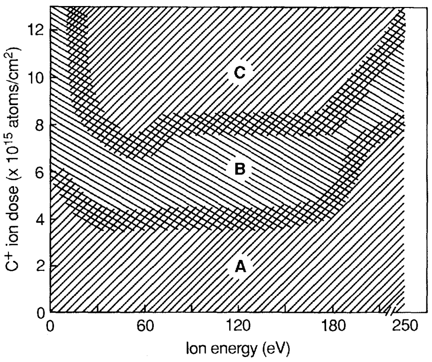

Fig. 3. Phase diagram as a function of C^+ ion dose and energy for deposition on Ni(111). Regions A, B, and C correspond to films that have the AES line shapes of Fig. 1, a, b, and c, respectively. The hatched regions represent transition zones from one form to another.

of a deposited diamondlike film and a graphite sample in Fig. 2 exhibit this distinction.

Several other techniques were used to characterize the carbon deposit. Ellipsometry measurements yielded refractive index values in the range from 2.25 to 2.57 with light incident at different angles. The spread in values is due to the varied thickness of the film over the area sampled. Pure diamond (*4*) has a refractive index of 2.41. UPS spectra exhibited a broad structure at 7.7 eV that corresponds to the ionization of tetrahedrally bonded carbon sp^3 atomic orbitals and there is a recession of the occupied density of states near the Fermi level. The carbon 1*s* line is observed in the XPS spectrum and the associated energy loss features are characteristic of diamond (*11*); the notable π-plasmon loss of graphite is absent in the diamondlike spectrum, which confirms the absence of π-electrons. ELS spectra exhibited plasmon and energy loss features identical to those of diamond (*7*), which are distinctly different from those of graphite. The energy of the bulk plasmon loss at 32 eV is proportional to the valence electron density, from which atomic density can be calculated. By using the expression (*4*) for the relation between plasmon energy and electron density and noting that carbon has four valence electrons, a density of 1.8×10^{23} was calculated. The atomic densities of pure diamond and graphite are 1.77×10^{23} and 1.13×10^{23} atoms per cubic centimeter, respectively.

The characteristic carbon Auger line shapes have been used to map out a carbon phase diagram for C^+ deposition on Ni(111) as a function of C^+ ion dose and energy (Fig. 3). The AES line shape (Fig. 1d) evolves smoothly from that of Fig. 1c and it is not possible to assign an exact dose for the crossover point. Hence a phase corresponding to Fig. 1d has not been indicated in Fig. 3. For ion energies below 10 eV, the carbon line shapes do not evolve completely into the final structure of Fig. 1d. In the range from 30 to 175 eV, the transformations are nearly energy-independent. This is the optimum energy for diamond film deposition. For energies greater than 180 eV, there is a sharp increase in the dose necessary to attain the different phases. In this region, the increasing significance of self-sputtering, lattice damage, and penetration by the C^+ ions is responsible for this phenomenon. For carbon deposition on Si(100) and gold surfaces, the doses necessary to achieve the same transitions as in Fig. 3 were higher than those on Ni(111). This sensitivity to the type of substrate surface arises from the intimate carbide registry with the surface.

The diamondlike films were analyzed for their composition and reactivities. Survey Auger scans revealed less than 1% of oxygen, nitrogen, and sulfur; the hydrogen content is expected to be insignificant as a result of the vacuum conditions used. An Auger depth concentration profile exhibited a sharp film-substrate interface. Oxygen chemisorption was examined on both the diamondlike film and a graphite sample. Exposure to O_2 resulted in a significant initial oxygen uptake (~40% surface coverage) by the graphite film, but only minor uptake (~10% surface coverage) by the diamondlike film. The ability of the films to resist sputtering by low-energy ions was also tested. The sputtering cross section with O^+ ions was ~1.9 Å^2 and was independent of energy in the range from 20 to 300 eV; the carbide sputtering yield in the same range is a factor of 2 higher. Sputtering by Ne^+ and Ar^+ ions was negligible at 20 eV and increased to only ~0.05 Å^2 at 300 eV. The spectral features are stable to ~350°C and complete transformation to graphic features occurs at 450° to 470°C.

Diamond is a metastable allotrope of carbon that requires activation energy for formation. The energy deposited by the impinging C^+ can result in the formation of metastable phases. The C^+ ions are efficiently neutralized before impact with the surface (*12*). These nascent neutral carbon atoms cause temporal agitations near the impact site. By using a simple model for thermal spikes (*13*), estimates for 100 eV carbon atoms impinging on a carbonaceous surface predict a localized (20 Å radius) spike with maximum temperature in the range from 10^3 to 10^4 K and a lifetime of the rapidly collapsing spike of the order of $\sim 10^{-11}$ seconds. These estimates show that a localized, transient, high-temperature environment can be produced and that the conditions prevail for time periods sufficient to allow for vibration and migration over short distances. The high quenching rates ($\sim 10^{14}$ K/sec) associated with the collapse of the spikes provide necessary conditions for trapping material in metastable phases. The energy is qualitatively explained by this model. If the energy is too low (<10 eV), spike conditions are not sufficient to allow the migration and rearrangement necessary for obtaining the metastable structure. If the energy is too high, severe damage is created over a large region; the migration distances for recombination of vacancy-intersitial pairs will be long and corresponding time periods may be longer than the quenching time of the thermal spike. Also, for energies greater than 100 eV, self-sputtering by impingent C^+ ions becomes nonnegligible. The fact that the initially deposited layer on the gold surface has the spectral features of a chemically bonded carbide structure emphasizes the extreme reactivity of the impinging C^+ ions. The chemical affinity of these incoming carbon ions must be sufficiently high such that they can react with an atomically clean gold surface to form Au-C surface carbide bonds.

REFERENCES AND NOTES

1. I. Stambler, *Res. Dev.* (August 1987), p. 41; J. McCormick, *ibid.* (July 1987), p. 44; G. Graff, *High Technol.* (April 1987), p. 44.
2. F. P. Bundy, H. M. Strong, R. H. Wentorf, Jr., in *Chemistry and Physics of Carbon*, P. L. Walker, Jr., and P. A. Thrower, Eds. (Dekker, New York, 1973), vol. 10, p. 213.
3. C. Weissmantel, in *Thin Films from Free Atoms and Particles*, K. J. Klabunde, Ed. (Academic Press, New York, 1985), p. 153.
4. T. Miyazawa, S. Misawa, S. Yoshida, S. Gonda, *J. Appl. Phys.* **55**, 188 (1984).
5. H. Kang, S. R. Kasi, J. W. Rabalais, unpublished results.
6. S. Craig *et al.*, *Surf. Sci.* **124**, 591 (1983).
7. P. G. Lurie and J. M. Wilson, *ibid.* **65**, 476 (1977).
8. A. K. Green and V. Rehn, *J. Vac. Sci. Technol.* **A1**, 1877 (1983).
9. B. B. Pate, *Surf. Sci.* **165**, 83 (1986).
10. T. J. Moravec and T. W. Orent, *J. Vac. Sci. Technol.* **18**, 226 (1981).
11. F. R. McFeely *et al.*, *Phys. Rev. B* **9**, 5268 (1974).
12. S. R. Kasi *et al.*, unpublished results.
13. F. Seitz and J. S. Koehler, *Progress in Solid State Physics* (Academic Press, New York, 1957), vol. 12, p. 30.
14. This material is based on work supported by the National Science Foundation under grants DMR-8610597 and CHE-8513966.

25 September 1987; accepted 15 December 1987

IRAS 14348–1447, an Ultraluminous Pair of Colliding, Gas-Rich Galaxies: The Birth of a Quasar?

D. B. SANDERS, N. Z. SCOVILLE, B. T. SOIFER

Ground-based observations of the object IRAS 14348–1447, which was discovered with the Infrared Astronomical Satellite, show that it is an extremely luminous colliding galaxy system that emits more than 95 percent of its energy at far-infrared wavelengths. IRAS 14348–1447, which is receeding from the sun at 8 percent of the speed of light, has a bolometric luminosity more than 100 times larger than that of our galaxy, and is therefore as luminous as optical quasars. New optical, infrared, and spectroscopic measurements suggest that the dominant luminosity source is a dust-enshrouded quasar. The fuel for the intense activity is an enormous supply of molecular gas. Carbon monoxide emission has been detected at a wavelength of 2.6 millimeters by means of a new, more sensitive receiver recently installed on the 12-meter telescope of the National Radio Astronomy Observatory. IRAS 14348–1447 is the most distant and luminous source of carbon monoxide line emission yet detected. The derived mass of interstellar molecular hydrogen is 6×10^{10} solar masses. This value is approximately 20 times that of the molecular gas content of the Milky Way and is similar to the largest masses of atomic hydrogen found in galaxies. A large mass of molecular gas may be a prerequisite for the formation of quasars during strong galactic collisions.

A FUNDAMENTAL DISCOVERY OF THE Infrared Astronomical Satellite [IRAS (*1*)] has been the recognition of a class of luminous galaxies emitting the bulk of their energy at infrared wavelengths (*2*). At bolometric luminosities above 10^{10} $L_\odot$ (equivalent to the total energy emitted by spiral galaxies like the Milky Way; $L_\odot$ is the luminosity of the sun) the space density of infrared galaxies in the "local" universe (*3*) is comparable to, or greater than, that of active and starburst galaxies, and at the highest luminosities ($\geq 10^{12}\ L_\odot$) the space density of "ultraluminous" infrared galaxies is larger than that of optically selected quasars (*4*). It has been proposed that ultraluminous infrared galaxies are, in fact, dust-enshrouded quasars (*5*). The trigger for this activity is the violent collision or merger of gas-rich spiral galaxies, an event that initially causes a violent starburst (that is, a transient period of rapid star formation), with the subsequent formation of the dust-enshrouded quasar. There has been mounting evidence in recent years that galaxy collisions play an important role in both luminous starbursts and in the formation of some quasars (*6*). However, it is through the subsequent detailed ground-based study of the high-luminosity infrared galaxies detected by IRAS that a more complete picture is emerging of the link between starbursts and quasars. In this report we present data gathered at several wavelengths that give a relatively comprehensive picture of one of the most spectacular ultraluminous infrared objects, IRAS 14348–1447. Of particular importance is the detection of the 2.6-mm line of carbon monoxide, which allows a determination of the total amount of molecular gas in this object.

The observations of IRAS 14348–1447 that are presented here are part of a larger program to study the brightest infrared galaxies detected by IRAS [the IRAS Bright Galaxy Survey (*7*)]. The data collected as part of this survey include optical, near infrared, and radio observations designed to provide as complete a picture as possible of the distribution of emitted radiation over a wide range of the electromagnetic spectrum. In addition, observations of the 21-cm line of atomic hydrogen (H I) and the 2.6-mm line of CO provide a measure of the total neutral gas content, a measurement that is important for assessing the total amount of fuel available for star formation, the formation of exotic nuclear sources such as a massive black hole, or both.

One of the most important initial results of this survey has been the discovery that infrared galaxies seem to show a morphological progression toward more strongly interacting pairs of galaxies as the luminosity of the system increases (*5*). Below 10^{11} $L_\odot$ the vast majority of the infrared objects are isolated galaxies. They appear to be powered by star formation, which is fueled by an abundant supply of molecular gas similar to what occurs in the disks of normal late-type spiral galaxies like the Milky Way. At higher luminosities there is a dramatic increase in the number of interacting systems and the incidence of dominant nonthermal nuclear emission. To date, all of these higher luminosity objects that have been observed in the 2.6-mm CO line show evidence for abundant molecular gas supplies and thus appear to be powered both by luminous starbursts and an active nucleus (*8*, *9*). At the highest luminosities ($\geq 10^{12}\ L_\odot$) the data to date have been less complete, but the preliminary indication was that all of the objects were strongly interacting galaxies powered by a dominant nonthermal source (*5*).

The highest redshift object in the IRAS Bright Galaxy Survey is IRAS 14348–1447 at a distance of approximately 330 megaparsecs (Mpc) (*3*). Figure 1 shows an optical charge-coupled detector (CCD) image of IRAS 14348–1447 obtained with the Palomar 1.5-m telescope (*10*). The isophotal map reveals a double nucleus in addition to an extended disk that is warped on the northeast side. The angular separation between the two nuclei is 4 arc sec, which corresponds to a distance of 10 kpc. The brighter nucleus is to the southwest. The color image in Fig. 2 shows these features more clearly. The total luminosity of the system is equivalent to the bolometric lumi-

---

D. B. Sanders, B. T. Soifer, Palomar Observatory, California Institute of Technology, Pasadena, CA 91125.
N. Z. Scoville, Owens Valley Radio Observatory, California Institute of Technology, Pasadena, CA 91125.